Analysis and Optimization of Pilot Symbol-Assisted Rake Receivers for DS-CDMA Systems

Tao Cui, *Student Member, IEEE*, and Chintha Tellambura, *Senior Member, IEEE*

***Abstract*—The effect of imperfect channel estimation (CE) on the performance of pilot-symbol-assisted modulation (PSAM) and MRC rake reception over time- or frequency-selective fading channels with either a uniform power delay profile (UPDP) or a nonuniform power delay profile (NPDP) is investigated. For time-selective channels, a Wiener filter or linear minimum mean square error (LMMSE) filter for CE is considered, and a closed-form asymptotic expression for the mean square error (MSE) when the number of pilots used for CE approaches infinity is derived. In high signal-to-noise ratio (SNR), the MSE becomes independent of the channel Doppler spectrum. A characteristic function method is used to derive new closed-form expressions for the bit error rate (BER) of rake receivers in UPDP and NPDP channels. The results are extended to two-dimensional (2-D) rake receivers. The pilot-symbol spacing and pilot-to-data power ratio are optimized by minimizing the BER. For UPDP channels, elegant results are obtained in the asymptotic case. Furthermore, robust spacing design criteria are derived for the maximum Doppler frequency.**

***Index Terms*—Channel estimation (CE), direct-sequence code-division multiple access (DS-CDMA), maximal ratio combining (MRC), Wiener filter.**

I. Introduction

WIDEBAND direct-sequence (DS) code-division multiple access (CDMA) with pilot-assisted coherent detection has been proposed as the basis for next-generation cellular systems [1]. A coherent system requires channel-estimation algorithms that track time-varying mobile radio channels. For this purpose, pilot symbols are transmitted along with data symbols. Pilot-symbol-assisted modulation (PSAM) [2] and pilot-channel-assisted modulation (PCAM) [3] have thus been proposed for the downlink in DS-CDMA systems. However, because PSAM and PCAM channel estimates are not perfect, an overall performance loss may ensue.

Rake receivers that employ coherent detection with maximal ratio combining (MRC) are thus popular in DS-CDMA systems [2]–[4]. To optimize PSAM and PCAM in conjunction with MRC and rake reception, the loss due to imperfect channel estimation must be quantified. In channels with uniform power delay profile (UPDP), the bit error rate (BER) of M-ary phase-shift keying (M-PSK) with channel-estimation errors has been derived in [5, App. C, pp. 949–961]. In [4], the influence of channel-estimation errors on the performance of a DS-CDMA system over a time-varying channel is investigated, where a simple average channel estimator is used.

On the other hand, the optimal pilot spacing for PSAM using a Wiener channel-estimation filter is obtained numerically in [6] for a flat fading channel. The number of pilot symbols for MRC is optimized in [7] using a clairvoyant channel estimator. For static fading channel and binary phase-shift keying (BPSK), the optimal pilot-symbol spacing in PSAM [2] and the optimal pilot-to-data power ratio (PDR) in PCAM [3] are designed for DS-CDMA systems by applying the results in [5, App. C, pp. 949–961]. The PDR in PCAM is optimized in [8] based on a large system analysis of a coded DS-CDMA system. However, because all of those papers use the well-known results from Proakis [5, App. C, pp. 949–961], their results hold for UPDP channels only. Only Benthin and Kammeyer [4], and Cavers [6] consider time-varying channels, but neither of them considers explicit optimal pilot design. To the best of our knowledge, a complete investigation of the effect of channel-estimation errors on the performance of MRC over nonuniform power delay profile (NPDP) channels along with pilot-symbol optimization is not available in the literature.

In this paper, we analyze the effect of imperfect channel estimation on the performance of rake reception with MRC and optimize the pilot-symbol spacing and PDR for DS-CDMA systems with PSAM. However, our results can readily be extended to optimizing PDR in PCAM as in [3] and [8], and other systems employing MRC and PSAM [2], [6]. For time-selective channels, we consider a Wiener filter or a linear minimum mean square error (LMMSE) filter for channel estimation and derive a closed-form asymptotic expression for the mean square error (MSE) when the number of pilots used for channel estimation approaches infinity. In high signal-to-noise ratio (SNR), the MSE becomes independent of the channel Doppler spectrum. We derive the BER of an MRC rake receiver in the presence of channel-estimation errors for both UPDP channels and NPDP channels, and our approach differs from [5, App. C, pp. 949–961]. We also extend the result to the two-dimensional (2-D) rake receiver. The pilot-symbol spacing is optimized by minimizing the BER in both the UPDP and NPDP channels. In UPDP channels, a closed-form expression is derived for the optimal pilot-symbol spacing and PDR in terms of Doppler frequency, SNR, and the number of channel paths; a robust

Manuscript received May 13, 2005; revised September 19, 2005 and December 4, 2005. This work was supported in part by the Natural Sciences and Engineering Research Council of Canada, the Informatics Circle of Research Excellence, and the Alberta Ingenuity Fund. This paper was presented in part at the IEEE Global Telecommunications Conference 2004, TX, November 2004. The review of this paper was coordinated by Dr. O. C. Ugweje.

T. Cui was with the Department of Electrical and Computer Engineering, University of Alberta, Edmonton, AB T6G 2V4, Canada. He is now with the Department of Electrical Engineering, California Institute of Technology, Pasadena, CA 91125 USA (e-mail: taocui@caltech.edu).

C. Tellambura is with the Department of Electrical and Computer Engineering, University of Alberta, Edmonton, AB T6G 2V4, Canada (e-mail: chintha@ece.ualberta.ca).

Digital Object Identifier 10.1109/TVT.2006.877699

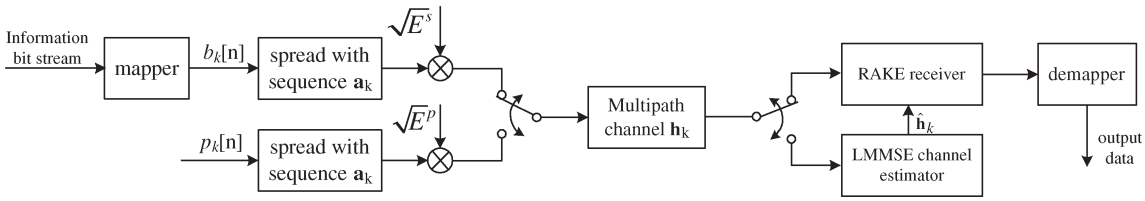

Fig. 1. Block diagram of the PSAM DS-CDMA system.

spacing is designed for the worst case Doppler frequency. Although our performance analysis results are fairly general, they are developed in the context of CDMA and PSAM.

The rest of this paper is organized as follows: In Section II, we briefly review the basic DS-CDMA system model and present the channel-estimation filters. The performance of MRC with imperfect channel estimation is analyzed in Section III. We optimize the pilot-symbol spacing in Section IV. Computer simulation results are given in Section V, and final conclusions are made in Section VI. We derive the asymptotic MSE for the LMMSE channel estimator in Appendix A. The performance analysis for the NPDP channel is derived in Appendix B.

Notation: Bold symbols denote matrices or vectors. $\Re(\cdot)$, $\Im(\cdot)$, $(\cdot)^*$, $(\cdot)^T$, $(\cdot)^H$, and $\mathrm{tr}(\cdot)$ denote real part, imaginary part, conjugate, transpose, conjugate transpose, and trace, respectively. The space of K-dimensional complex vectors is $\mathcal{C}^K$. A circularly complex Gaussian random variable (CGRV) of mean μ and variance σ^2 is denoted by $z \sim \mathcal{CN}(\mu, \sigma^2)$. The imaginary unit $\mathrm{j} = \sqrt{-1}$ and the $N \times N$ identity matrix is denoted by $\mathbf{I}_N$. A diagonal matrix formed by vector $\mathbf{A}$ is $\mathbf{A}_D$. The Kronecker delta function is given by $\delta(x) = 1$ if $x = 0$ and $\delta(x) = 0$ if $x \neq 0$. The unit-step function is given by $u(x) = 1$ if $x \geq 0$ and $u(x) = 0$ if $x < 0$.

II. System Model

We consider the downlink of an isolated DS-CDMA cell over a time- and frequency-selective channel. The system block diagram for a single user is shown in Fig. 1. The system is assumed to be synchronous and with K users, each with processing gain N. The spreading sequence of the kth user is denoted by the $N \times 1$ vector $\mathbf{a}_k$ with common chip rate $1/T_c$, and the information symbol transmitted in the nth symbol interval is $b_k[n]$ with information symbol rate $1/T_s$, where $T_s = NT_c$. Rectangular pulse shaping is used. In practical systems, $\mathbf{a}_k$ is time varying and is the multiplication of a channelization code and a scrambling code. The information symbol $b_k[n]$ is chosen from a finite alphabet constellation $\mathcal{Q}$ with unity average energy. Typically, for BPSK, $\mathcal{Q} = \{-1, 1\}$.

We now consider PSAM, in which the pilot symbols p are transmitted periodically with the pilot spacing M and are subject to $|p|^2 = 1$. Therefore, the baseband transmitted signal of the nth symbol of the kth user $(k = 1, \ldots, K)$ is given by

$$\mathbf{x}_k[n] = \begin{cases} \sqrt{E_k^p}\mathbf{a}_k p_k[n], & n = iM \\ \sqrt{E_k^s}\mathbf{a}_k b_k[n], & \text{otherwise} \end{cases} \tag{1}$$

where E_k^p and E_k^s are the transmitted powers for the pilots and information symbols, respectively.

The user signal is transmitted over a frequency-selective multipath Rayleigh-fading channel, which can be modeled as a finite-length tapped delay line [5]. The lowpass impulse response for a time-variant frequency-selective channel is given by [5, p. 841]

$$h(\tau; t) = \sum_{l=0}^{L-1} h_l(t)\delta(\tau - \tau_l) \tag{2}$$

where $h_l(t) \sim \mathcal{CN}(0, \sigma_l^2)$, τ_l is the delay of the lth tap, and L is the number of channel paths. Both σ_l^2 and τ_l define the power delay profile (PDP) of the channel. To simplify our analysis, it is assumed that the PDP is constant. For brevity, we consider two PDPs, namely 1) the UPDP and 2) the exponential power delay profile (EPDP). They can be expressed as

$$\sigma_l^2 = \begin{cases} C, & \text{UPDP} \\ Ce^{-\rho l}, & \text{EPDP} \end{cases} \tag{3}$$

where $\rho = \tau_0/\tau_{\mathrm{rms}}$, τ_0 is the time duration between two consecutive discrete taps, τ_{rms} is the root-mean-square (rms) delay spread, and C is the constant term that normalizes the power to unity. However, our analytical results developed in Section III can handle any NPDP channels.

We assume that $h_l(t)$ has the same normalized correlation function $\phi^c(\Delta t)$ (superscript c emphasizes continuous delays rather than discrete delays) and that the channel taps are independent ($E\{h_{l_1}(t)h_{l_2}^*(t)\} = 0$ for $l_1 \neq l_2$). The autocorrelation function of $h_l(t)$ is given by

$$\phi_l^c(\Delta t) = E\left\{h_l(t + \Delta t)h_l^*(t)\right\} = \sigma_l^2\phi^c(\Delta t). \tag{4}$$

Typically, for Jakes' model [9], $\phi^c(\Delta t) = J_0(2\pi f_d \Delta t)$, where $J_0(\cdot)$ denotes the zeroth-order Bessel function of the first kind and f_d is the maximum Doppler frequency in hertz.

We assume a quasi-static (QS) fading channel [10] that remains constant in each symbol interval T_s but may vary from symbol to symbol. The equivalent discrete channel model is

$$h[d; n] = \sum_{l=0}^{L-1} h_l[n]\delta[d - d_l] \tag{5}$$

where $h_l[n] = h_l(nT_s)$ and $d_l = \lfloor \tau_l/T_c \rceil$ is an integer ($\lfloor x \rceil$ is the integer close to x). Without loss of generality, it is assumed that $d_l = l$, which means that each subsequent path is delayed by one chip period. The autocorrelation function of $h_l[n]$ is thus given by

$$\phi_l^d[m] = E\left\{h_l[n + m]h_l^*[n]\right\} = \phi_l^c(mT_s) = \sigma_l^2\phi^c(mT_s). \tag{6}$$

We next consider the performance of the first user without loss of generality because all user signals are transmitted over the same channel model (5). The first user's received signal for symbol n is

$$\mathbf{r}_1[n] = \left(\sum_{k=1}^{K} \left(\sum_{l=0}^{L-1} \sqrt{E_k} h_{k,l}[n] \mathbf{x}_k^{(l)}[n] \right) + \psi_k[n] \right) + \mathbf{w}[n] \tag{7}$$

where E_k is the received energy per symbol for the kth user, including both pilot and data symbols, $h_{k,l}[n]$ is the lth path channel gain for user k, $\mathbf{w}[n]$ is the $N \times 1$ vector of complex Gaussian noise samples with mean zero and variance σ_n^2, and $\mathbf{r}_1[n]$ is the $N \times 1$ vector received by user 1. The $N \times 1$ vector $\mathbf{x}_k^{(l)}[n]$ is a shifted version of $\mathbf{x}_k[n]$, given in (1), with the first l elements equal to zero and the remaining $N-l$ elements equal to the first $N-l$ elements of $\mathbf{x}_k[n]$. The vector $\psi_k[n]$ represents the intersymbol interference (ISI) from the $(n-1)$th symbol for the kth user caused by the frequency-selective channels. Therefore, only the first $L-1$ elements of $\psi_k[n]$ are nonzero.

The rake receiver first performs correlations using circularly shifted spreading sequences $\mathbf{a}_1^{(l)}$, for $l = 0, \ldots, L-1$, where $\mathbf{a}_1^{(l)}$ denotes the circular shift of $\mathbf{a}_1$ by l positions. The correlator outputs are given by $(l = 0, \ldots, L-1)$

$$\begin{aligned} r_l[n] &= \left(\mathbf{a}_1^{(l)}\right)^H \mathbf{r}_1[n] \\ &= \begin{cases} \sqrt{E_1^p} h_{1,l}[n] p_1[n] + w[n] + \mu[n] + \xi[n], & n = iM \\ \sqrt{E_1^s} h_{1,l}[n] b_1[n] + w[n] + \mu[n] + \xi[n], & \text{otherwise} \end{cases} \end{aligned} \tag{8}$$

where $w_l[n] = (\mathbf{a}_1^{(l)})^H \mathbf{w}[n]$ is a complex Gaussian variable with mean zero and variance σ_n^2, $\mu_l[n] = (\mathbf{a}_1^{(l)})^H \sum_{k=1}^{K} \psi_k[n]$ is the ISI, and $\xi_l[n]$ represents both interpath interference (IPI) and multiple-access interference (MAI) given by

$$\xi_l[n] = \sum_{k=1}^{K} \sum_{l=0}^{L-1} \sqrt{E_k} h_{k,l}[n] \left(\mathbf{a}_1^{(l)}\right)^H \mathbf{x}_k^{(l)}[n] - \sqrt{E_1} h_{1,l}[n] b_1[n]. \tag{9}$$

When N and K are large, $\mu_l[n]$ and $\xi_l[n]$ can be approximated as Gaussian [11], and (8) can be simplified as

$$r_l[n] = \begin{cases} \sqrt{E^p} h_l[n] p[n] + u_l[n], & n = iM \\ \sqrt{E^s} h_l[n] b[n] + u_l[n], & \text{otherwise} \end{cases} \qquad l = 0, \ldots, L-1 \tag{10}$$

where $u_l[n] = w_l[n] + \mu_l[n] + \xi_l[n]$ is complex Gaussian with zero mean and variance σ_u^2; we omit the user subscript for brevity. We assume that all user spreading sequences are mutually orthogonal, i.e., $\mathbf{a}_i^H \mathbf{a}_j = \delta(i-j)$. Moreover, as [5, p. 845], for pseudorandom sequences, $(\mathbf{a}_k^{(i)})^H \mathbf{a}_k^{(j)} \simeq \delta(i-j)$. Therefore, as will be shown in Section III, $\mu_l[n]$ and $\xi_l[n]$ do not affect the rake receiver performance in low SNR (SNR $<$ 15 dB) in a wideband CDMA (WCDMA) system. In high SNR, using Gaussian approximation on $\mu_l[n]$ and $\xi_l[n]$ [11], our results can be readily extended to systems with $\mu_l[n]$ and $\xi_l[n]$ by replacing σ_n^2 with σ_u^2. In this paper, we assume perfect knowledge of channel delay τ_l and L.

The coherent receiver comprises an LMMSE channel estimator and a rake demodulator. The channel gains $h_l[n]$ are estimated, and the information symbols are recovered using MRC.

A. Channel Estimation

We use a Wiener filter or an LMMSE channel estimator to estimate the time-varying channel. From (10), the frequency-selective channel is decoupled into L parallel subchannels in DS-CDMA systems. Therefore, we only show how to estimate the lth path, and the other paths can be obtained similarly. In the channel estimator, P pilot symbols are used, and they are stacked in a vector $\mathbf{x} = [p[-(\lceil P/2 \rceil - 1)M], \ldots, p[\lfloor P/2 \rfloor M]]^T$, where $\lceil x \rceil$ denotes the smallest integer greater than or equal to x and $\lfloor x \rfloor$ denotes the largest integer smaller than or equal to x. We define the $P \times 1$ vector $\mathbf{r}_l = [r_l[-(\lceil P/2 \rceil - 1)\rfloor M], \ldots, r_l[\lfloor P/2 \rfloor M]]^T$ corresponding to the pilot symbols. The channel gain at the mth symbol interval is estimated as

$$\hat{h}_l[m] = \mathbf{w}_l^H[m] \mathbf{r}_l, \qquad -\lceil P/2 \rceil M < m \le \lfloor P/2 \rfloor M \tag{11}$$

where $\mathbf{w}[m]$ is the optimal Wiener filter coefficients vector for the mth symbol. From the well-known Wiener filter theory [12], we define the $P \times 1$ cross-correlation vector as

$$\mathbf{q}_l[m] = E\{h_l^*[m] \mathbf{r}_l\} = \sqrt{E^p} \mathbf{X}_D \mathbf{c}_{d,p} \tag{12}$$

where $\mathbf{X}_D = \text{diag}\{\mathbf{x}\}$ and $\mathbf{c}_{d,p} = [\phi_l^d[m + (\lceil P/2 \rceil - 1)M], \ldots, \phi_l^d[m - \lfloor P/2 \rfloor M]]^T$.

The $P \times P$ autocorrelation matrix is defined as

$$\mathbf{R}_l[m] = E\left\{\mathbf{r}_l \mathbf{r}_l^H\right\} = E^p \mathbf{X}_D \mathbf{C}_h \mathbf{X}_D^H + \sigma_n^2 \mathbf{I}_P \tag{13}$$

where the channel correlation matrix $\mathbf{C}_h$ is given by

$$\mathbf{C}_h = \begin{bmatrix} \phi_l^d[0] & \phi_l^d[-M] & \cdots & \phi_l^d[-(P-1)M] \\ \phi_l^d[M] & \phi_l^d[0] & \cdots & \phi_l^d[-(P-2)M] \\ \vdots & \vdots & \ddots & \vdots \\ \phi_l^d[(P-1)M] & \phi_l^d[(P-2)M] & \cdots & \phi_l^d[0] \end{bmatrix}. \tag{14}$$

Finally, we can obtain

$$\mathbf{w}_l[m] = \mathbf{R}_l[m]^{-1} \mathbf{q}_l[m]. \tag{15}$$

The MSE of the LMMSE channel estimate is given by

$$\begin{aligned} \sigma_{l,\Delta h}^2[m] &= E\left\{ \left| h_l[m] - \hat{h}_l[m] \right|^2 \right\} \\ &= \sigma_l^2 - \mathbf{q}_l^H[m] \mathbf{R}_l^{-1}[m] \mathbf{q}_l[m] \\ &= \sigma_l^2 - \mathbf{c}_{d,p}^H \left(\mathbf{C}_h + \frac{\sigma_n^2}{E_p} \mathbf{I}_P \right)^{-1} \mathbf{c}_{d,p}. \end{aligned} \tag{16}$$

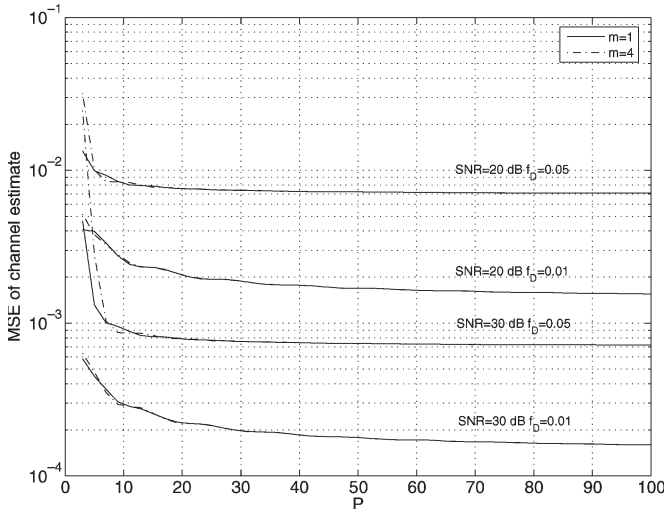

Fig. 2. MSE of the LMMSE channel estimate versus the number of pilot symbols P with different SNRs and f_Ds with $M = 7$.

From (16), $\sigma^2_{l,\Delta h}[m]$ does not depend on the specific value of $p[n]$. Therefore, $p[n]$ can be any value with unity power. For simplicity, we choose $p[n] = +1$. Note that if the powers of the pilot symbols are not the same, using the results in [13], it can be readily verified that given constant total power, the average MSE $\sum_{m=-(\lceil P/2\rceil-1)M}^{\lfloor P/2\rfloor M} \sigma^2_{l,\Delta h}[m]/P$ is minimized if and only if all of the pilot symbols have the same power. This verifies our equipower assumption for pilot symbols. However, $\sigma^2_{l,\Delta h}[m]$ depends on P in a complicated way. To simplify the optimization of pilots in Section IV, we consider the asymptotic MSE $\bar{\sigma}^2_{l,\Delta h}[m] = \lim_{P\to\infty} \sigma^2_{l,\Delta h}[m]$. From Appendix A, when $\sigma_n^2 \to 0$, we get an elegant result, i.e.,

$$\bar{\sigma}^2_{l,\Delta h} \simeq 2M f_D \frac{\sigma_n^2}{E^p}. \tag{17}$$

A remarkable property is that (17) does not depend on the specific Doppler spectrum $S_l^d(\omega)$. This property indicates that our pilot optimization using (17) is robust to the Doppler spectrum mismatch. In Fig. 2, we plot the value of $\sigma^2_{l,\Delta h}[m]$ as a function of P, for different m, SNR, and f_D with $M = 7$. For $f_D = 0.05$, after $P > 15$, $\sigma^2_{l,\Delta h}[m]$ becomes constant and is the same for different ms. For $f_D = 0.01$, $\sigma^2_{l,\Delta h}[m]$ becomes constant when $P > 60$. However, when $P > 10$, the MSEs for different ms are almost the same.

B. Data Detection

An MRC rake receiver is used with the Wiener or LMMSE channel estimator. MRC corrects the phase rotation caused by a fading channel and then combines the received signals of different paths proportional to the strength of each path. Given perfect channel estimates, MRC is optimal for minimizing BER [14]. When MRC is used with estimated channel gains, the nth information symbol $b[n]$ can be detected as

$$b[n] = \arg\min_{b\in Q} \left| b - \frac{\sum_{l=0}^{L-1} \hat{h}_l^*[n] r_l[n]}{\sum_{l=0}^{L-1} \left|\hat{h}_l[n]\right|^2} \right|^2 \tag{18}$$

where $\hat{h}_l[n]$ is the estimated channel gain using (11). Specifically, for BPSK, (18) can be simplified as

$$b[n] = \text{sign}\left[\Re\left(\sum_{l=0}^{L-1} \hat{h}_l^*[n] r_l[n] \right) \right] \tag{19}$$

where $\text{sign}(\cdot)$ takes the sign of the operator.

Due to the channel-estimation error in $\hat{h}_l[n]$, the MRC rule (18) is not optimal because the performance of MRC will be impaired by the channel-estimation errors. To improve the receiver performance, data detection and channel estimation can be jointly performed. Such a simple receiver can use decision direct technique, where the estimated data symbols are fed back to the channel estimator (11). The updated channel estimates are used to improve the performance of MRC in (18).

III. Performance of MRC With Imperfect Channel Estimation

From (11), $\hat{h}_l[n]$ is also complex Gaussian with mean zero and variance $\sigma_l^2 - \sigma^2_{l,\Delta h}$. In this section, we will derive the BER of an MRC rake receiver with channel-estimation errors for both UPDP channels and NPDP channels.

A. UPDP Channels

We consider the BER of the nth symbol. The BER of MRC with Gaussian-distributed weighting errors for BPSK in UPDP has been derived by Proakis [5, App. C, pp. 949–961], which is given by

$$P_{2b} = \frac{1}{2}\left[1 - \mu \sum_{k=0}^{L-1} \binom{2k}{k} \left(\frac{1-\mu^2}{4} \right)^k \right] \tag{20}$$

where μ is the cross-correlation coefficient of the receiver correlator output samples and the channel estimates at the nth symbol from (11).

We denote Y_k as $\hat{h}_k$ and X_k as r_k. The output of the rake receiver can be expressed as

$$z = \sum_{k=0}^{L-1} \hat{h}_k^* r_k = \sum_{k=0}^{L-1} X_k Y_k^*. \tag{21}$$

Then, μ is given by [5, p. 952]

$$\begin{aligned} m_{xx} &= E\left(|X_k|^2\right) \\ m_{yy} &= E\left(|Y_k|^2\right) \\ m_{xy} &= E\left(X_k Y_k^*\right) \\ \mu &= \frac{m_{xy}}{\sqrt{m_{xx} m_{yy}}}. \end{aligned} \tag{22}$$

Equation (20) is derived assuming all pairs (X_k, Y_k) are independent and identically distributed. This classical method is due to Proakis [5, App. C, pp. 949–961]. He derives the joint characteristic function (chf) of the real and imaginary parts of $X_k Y_k^*$, raises the chf to the power L, Fourier transforms the results, converts from rectangular to polar form, and finally integrates over the amplitude variable. The result gives the probability density function (pdf) of the decision phase variable. However, this approach fails when (X_k, Y_k) are distributed nonidentically.

B. NPDP Channels

In this subsection, we derive the BER of a rake receiver in NPDP channels using a different approach than that used in the UPDP case given by Proakis [5, App. C, pp. 949–961]. We still use the previously defined symbols.

The error probability of BPSK is derived in Appendix B as

$$P_{2b} = (-1)^{L+1} \sum_{k=0}^{L-1} \frac{v_{k1}}{v_{k1} + v_{k2}} \prod_{l=0, l\neq k}^{L-1} \frac{v_{l1} v_{l2}}{(v_{k2} + v_{l1})(v_{k2} - v_{l2})}. \tag{23}$$

When the channel has a UPDP, the BER expression (23) reduces to

$$P_{2b} = \frac{1}{(1 + v_2/v_1)^{2L-1}} \sum_{k=0}^{L-1} \binom{2L-1}{k} \left(\frac{v_2}{v_1}\right)^k \tag{24}$$

where $v_2 = v_{k2}$ for all k and $v_1 = v_{k1}$ for all k.

Because QPSK is equivalent to two independent BPSK channels, the symbol error probability is

$$P_{4s} = 1 - (1 - P_{2b})^2 = 2P_{2b} - P_{2b}^2 \tag{25}$$

where P_{2b} is given in (74). If the information bits are Gray mapped into QPSK and quadratic amplitude modulation (4QAM), QPSK and 4QAM have the same BER. Therefore, we try to find the BER of 4QAM with

$$\begin{aligned} 00 &\to \frac{\sqrt{2}}{2} + \mathrm{j}\frac{\sqrt{2}}{2}, \qquad 01 \to -\frac{\sqrt{2}}{2} + \mathrm{j}\frac{\sqrt{2}}{2} \\ 11 &\to -\frac{\sqrt{2}}{2} - \mathrm{j}\frac{\sqrt{2}}{2}, \quad 10 \to \frac{\sqrt{2}}{2} - \mathrm{j}\frac{\sqrt{2}}{2}. \end{aligned} \tag{26}$$

Assuming 00 is transmitted, the BER of 4QAM is given by

$$P_{4b} = \frac{1}{2}\left[P(D_R < 0) + P(D_I < 0)\right] \tag{27}$$

where D_R is given by (65) and D_I is

$$D_I = 2\Im\left\{\sum_{k=0}^{L-1} X_k Y_k^*\right\} = \sum_{k=0}^{L-1} -\mathrm{j}X_k Y_k^* + \mathrm{j}X_k^* Y_k. \tag{28}$$

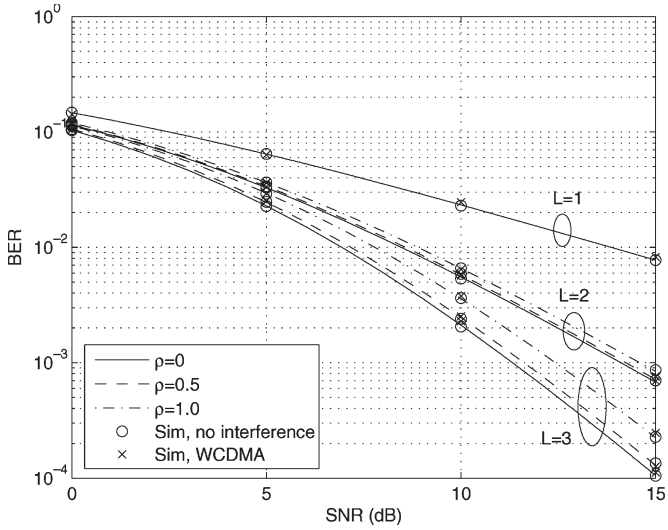

Fig. 3. BER versus SNR with different $\rho = \tau_0/\tau_{\mathrm{rms}}$ and L in a BPSK WCDMA downlink.

Following the same approach from (66)–(74), we can find $P(D_R < 0)$ and $P(D_I < 0)$ in closed form, where $P(D_I < 0)$ $C = -\mathrm{j}$ in (66).

Remarks:

1) Although (24) appears different from (20) given by [5, App. C, pp. 949–961], it can be verified that they are equivalent from both analysis and simulation. Therefore, this special case partly affirms the correctness of (74). Equation (74) also gives the BER for MRC with no channel-estimation errors in NPDP channels.
2) For M-ary QAM (MQAM)-modulated systems with Gray mapping, the closed form of BER for UPDP channels has been derived in [15]. For NPDP channels, the closed-form BER can be readily obtained similarly to that of 4QAM.

We briefly compare the analytical results with the simulation results for a BPSK WCDMA downlink. The channelization codes are Walsh codes with a processing gain $N = 256$ [16]. $K = 3$ synchronous users are simulated with the same scrambling code, a Gold code generated by two polynomials, namely 1) $P_1(X) = 1 + X^7 + X^{18}$ and 2) $P_2(X) = 1 + X^5 + X^7 + X^{10} + X^{18}$ [16]. The channel has an EPDP (3). The SNR for the first user is defined as E_1^d/N_0.

Fig. 3 shows that the theoretical BER given by (74) is consistent with the simulation results without interference when the PDP have a different ρ. Perfect channel state information (CSI) is assumed in the simulation. With the increase of ρ, the performance of MRC will degrade due to frequency-selective fading. When ρ approaches zero, (74) coincides with (20) and (24). With the increase of the channel length L, the performance degradation due to frequency selectivity becomes more severe. The WCDMA-downlink simulation results also agree with the analytical results. The performance degradation by $\mu[n]$ and $\xi[n]$ is negligible in low SNR, which is usually the case in practice. Therefore, we ignore $\mu[n]$ and $\xi[n]$ in Section IV.

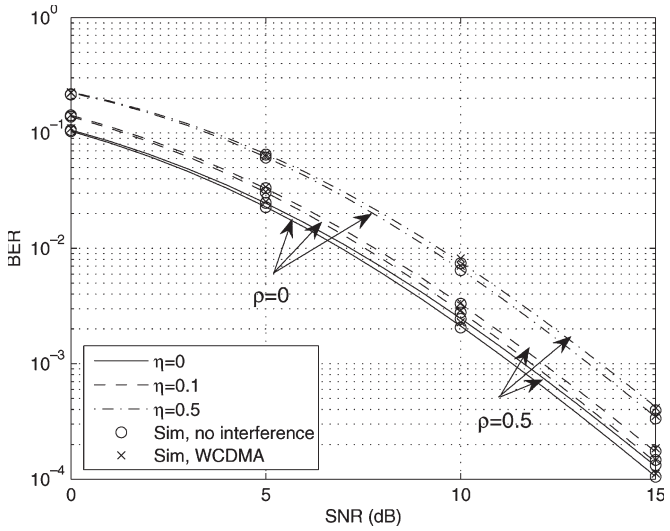

Fig. 4. BER versus SNR with different $\rho = \tau_0/\tau_{\rm rms}$, η, and fixed $L = 3$ in a BPSK WCDMA downlink.

Calculation has shown that for $L = 3$ and $\rho = 0$, $E\{|\mu_l[n] + \xi_l[n]|^2\} = 0.0157$ for $l = 0, 1, 2$, which will cause an error floor in high SNR.

From (17), $\bar{\sigma}^2_{l,\Delta h}$ only depends on σ^2_n. Therefore, we define $\sigma^2_{l,\Delta h} = \eta\sigma^2_n$, where η denotes the effect of channel-estimation errors. Fig. 4 shows the performance loss due to the channel-estimation error when $L = 3$ under different ρ and η. The BER can be degraded severely by the channel-estimation error. When $\eta = 0.5$, the performance loss can be as large as 3 dB. The simulation results with and without interference agree with the analytical results as well.

C. 2-D Rake Receivers

We now extend our previous analysis of MRC with imperfect channel estimation to a 2-D rake receiver with an A-elements antenna array [17], [18]. For simplicity, we assume that the channels between the transmitter and each antenna of the receiver have L branches as per (2) and identical statistics. Therefore, the receiver is composed of L rake branches. The 2-D rake receiver employs MRC in both the space and time domains.

We assume that the separation between the A antennas is large enough so that the received signals at each antenna are mutually independent. Ignoring the ISI, the received signal by the first user at the ath antenna during the nth interval can be expressed as

$$\mathbf{r}_{1,a}[n] = \sum_{k=1}^{K}\sum_{l=0}^{L-1}\sqrt{E_k}h_{k,a,l}[n]\mathbf{x}_k^{(l)}[n] + \mathbf{w}_a[n] \qquad a = 1, \ldots, A \quad (29)$$

where $h_{k,a,l}$ denotes the lth channel gain between the kth user and ath receiver antennas, and $\mathbf{w}_a[n]$ is the additive noise vector. After despreading, similar to (10), we get

$$r_{a,l}[n] = \left(\mathbf{a}_1^{(l)}\right)^H \mathbf{r}_{1,a}[n] = \begin{cases} \sqrt{E_1^p}h_{a,l}[n]p[n] + u_{a,l}[n], & n = iM \\ \sqrt{E_1^s}h_{a,l}[n]b[n] + u_{a,l}[n], & \text{otherwise} \end{cases} \qquad l = 0, \ldots, L-1, \quad a = 1, \ldots, A \quad (30)$$

where the first-user subscript is omitted for brevity. The LMMSE channel estimator for $h_{a,l}[n]$ can be obtained as (11) using pilot symbols, and the channel estimate is denoted by $\hat{h}_{a,l}[n]$.

As before, the estimated channel gains can be used with the 2-D rake receiver. Using the maximum-likelihood (ML) principle, the data detector for the nth information symbol can then be derived as

$$b[n] = \arg\min_{b\in\mathcal{Q}} \left| b - \frac{\sum_{a=1}^{A}\sum_{l=0}^{L-1}\hat{h}^*_{a,l}[n]r_{a,l}[n]}{\sum_{a=1}^{A}\sum_{l=0}^{L-1}\left|\hat{h}_{a,l}[n]\right|^2} \right|^2. \quad (31)$$

Following the derivation of (74), we get a similar result as

$$P_{2b} = (-1)^{L+1}\sum_{a=1}^{A}\sum_{k=0}^{L-1}\frac{v_{ak1}}{v_{ak1}+v_{ak2}} \prod_{j=1,\mathrm{j}\neq a}^{A}\prod_{l=0,l\neq k}^{L-1}\frac{v_{jl1}v_{jl2}}{(v_{ik2}+v_{jl1})(v_{ik2}-v_{jl2})}. \quad (32)$$

IV. Optimizing Pilot-Symbol Spacing and Power

We next optimize the pilot-symbol spacing and PDR by minimizing the BER. While we take BPSK systems as an example, other modulations can be optimized similarly. The existence of the optimal values of these parameters can be understood by knowing the fact that increasing the power allocated to pilot symbols improves the channel-estimation accuracy and thus may decrease the output BER. On the other hand, given fixed total power, an increase of the pilot energy decreases the SNR, and thus, the BER will increase.

A. UPDP Channels

To compute the BER, we need to obtain μ in (20). Let the channel power gains be $\sigma_l^2 = \sigma_h^2$, for $l = 0, \ldots, L-1$. From (10), we have

$$m_{xx} = E\left\{|r_k|^2\right\} = E^s\sigma_h^2 + \sigma_n^2. \quad (33)$$

With the LMMSE channel estimator, in the nth symbol interval, we find

$$m_{yy} = E\left\{|\hat{h}_k|^2\right\} = \mathbf{q}_l^H[n]\mathbf{R}_l^{-1}[n]\mathbf{q}_l[n] \quad (34)$$

and

$$m_{xy} = E\left\{r_k\hat{h}_k^*\right\} = \sqrt{E^s}b[n]\mathbf{q}_l^H[n]\mathbf{R}_l^{-1}[n]\mathbf{q}_l[n] \quad (35)$$

where (34) follows from (16), and $\mathbf{q}_l$ and $\mathbf{R}_l$ are defined in (16). Assuming $b[n] = +1$, we get

$$\mu = \frac{m_{xy}}{\sqrt{m_{xx}m_{yy}}} = \frac{\sqrt{E^s}\mathbf{q}_l^H[n]\mathbf{R}_l^{-1}[n]\mathbf{q}_l[n]}{\sqrt{\left(E^s\sigma_h^2 + \sigma_n^2\right)\mathbf{q}_l^H[n]\mathbf{R}_l^{-1}[n]\mathbf{q}_l[n]}}. \quad (36)$$

However, μ in (36) depends on the time index n. Thus, the pilot-symbol design should be optimized to minimize the average BER $\bar{P}_b = \sum_{n=1}^{N} P_{2b}(n)/N$, where N is the number of symbols used for averaging and P_{2b} is given in (20). To remove the BER's dependence on n, we evaluate the asymptotic BER when $P \to \infty$. Comparing (59) with (16), we find

$$\lim_{P\to\infty} \mathbf{q}_l^H[n]\mathbf{R}_l^{-1}[n]\mathbf{q}_l[n] = \sigma_h^2 - \bar{\sigma}_{l,\Delta h}^2 \quad (37)$$

where $\bar{\sigma}_{l,\Delta h}^2$ is given in (60). Substituting (37) into (36), we have

$$\mu = \sqrt{\frac{E^s\left(\sigma_h^2 - \bar{\sigma}_{l,\Delta h}^2\right)}{E^s\sigma_h^2 + \sigma_n^2}}. \quad (38)$$

Note that μ in (38) does not depend on time index n. For Jakes' model, (62) can be substituted into (38). Assuming the average power per information symbol is $\mathcal{E}$, the total power allocated for the M symbols is $(M-1)\mathcal{E}$ or $(M-1)E^s + E^p = (M-1)\mathcal{E}$. Let the percentage of power allocated to information symbols be denoted by γ. We then have $E^s = \gamma\mathcal{E}$ and $E^p = (1-\gamma)(M-1)\mathcal{E}$. Substituting (17), E^s, and E^p into (38), we obtain

$$\mu(\gamma, M) = \sqrt{\frac{\gamma\mathcal{E}\left(\sigma_h^2 - 2Mf_D\frac{\sigma_n^2}{(1-\gamma)(M-1)}\mathcal{E}\right)}{\gamma\mathcal{E}\sigma_h^2 + \sigma_n^2}}. \quad (39)$$

On the other hand, it can be readily proved that P_{2b} in (20) is a monotonously decreasing function of μ. Therefore, minimizing BER P_{2b} is equivalent to maximizing μ. In (39), fixing γ, μ increases with the increase of M. If M is increased from $m-1$ to m, we can always find a γ_m so that $\mu(\gamma_m, m) \geq \mu(\gamma_{m-1}, m) \geq \mu(\gamma_{m-1}, m-1)$. Hence, M should be chosen as large as possible. Considering (58), we conclude that the optimal pilot-symbol spacing is

$$M_{\text{opt}} = \left\lfloor \frac{1}{2f_D} \right\rfloor - 1 \quad (40)$$

where 1 is subtracted to avoid the aliasing caused by the nonideal bandlimited Doppler spectrum.

The optimal γ can be found by taking the partial derivative of $\mu(\gamma, M_{\text{opt}})$ over γ. We find

$$\gamma_{\text{opt}} = \frac{\sqrt{4ac\left[(a+c)b - b^2\right]} - 2ac}{2a(b-c)} \quad (41)$$

where

$$a = \mathcal{E}\sigma_h^2, \quad b = \frac{2M_{\text{opt}}f_D\sigma_n^2}{M_{\text{opt}} - 1}, \quad c = \sigma_n^2. \quad (42)$$

To further gain insight into the optimal pilot-symbol design problem, we consider the case when $\sigma_n^2 \to 0$. When $\sigma_n^2 \to 0$, (41) reduces to

$$\gamma_{\text{opt}} \simeq \frac{1}{\sqrt{\frac{2M_{\text{opt}}f_D}{M_{\text{opt}}-1}} + 1}. \quad (43)$$

Both (41) and (43) are fairly simple and independent of any specific Doppler spectrum and SNR. Thus, they are useful for designing practical systems. However, both (40) and (43) need the knowledge of Doppler frequency f_D, which may not be obtained accurately in practical systems. Robust design to the mismatch of f_D should be considered. Note that substituting (43) into (39), we can get

$$\mu(f_D) = \sqrt{\frac{\mathcal{E}\sigma_h^2 - \sqrt{\frac{2M_{\text{opt}}f_D}{M_{\text{opt}}-1}}\sigma_n^2}{\mathcal{E}\sigma_h^2 + \left(\sqrt{\frac{2M_{\text{opt}}f_D}{M_{\text{opt}}-1}} + 1\right)\sigma_n^2}}. \quad (44)$$

We readily see that $\mu(f_D)$ is a monotonously decreasing function of f_D. If the maximum normalized Doppler frequency is $f_{\max}$, $\mu(f_{\max})$ achieves the maximum BER. Therefore, M and γ should be designed using $f_{\max}$ to gain robustness to the mismatch of f_D or when f_D is unknown.

In practical systems, equipower PSAM is usually used to simplify the transmitter design. For equipower PSAM, $E^s = E^p = (M-1)\mathcal{E}/M$ or $\gamma = (M-1)/M$. Equation (39) reduces to

$$\mu(M) = \sqrt{\frac{(M-1)\mathcal{E}\sigma_h^2 - 2M^2f_D\sigma_n^2}{(M-1)\mathcal{E}\sigma_h^2 + M\sigma_n^2}}. \quad (45)$$

By taking the partial derivative of $\mu(M)$ over M and setting the results equal to zero, we get

$$M_{\text{opt}} = \frac{2ac + \sqrt{4a^2c^2 + 4ab(a+b)c}}{2(a+b)c} \quad (46)$$

where

$$a = \mathcal{E}\sigma_h^2, \quad b = \sigma_n^2, \quad c = 2f_D\sigma_n^2. \quad (47)$$

When $\sigma_n^2 \to 0$, (46) can be simplified to

$$M_{\text{opt}} = 1 + \sqrt{1 + \frac{1}{2f_D}}. \quad (48)$$

The two integers $\lfloor M_{\text{opt}} \rfloor$ and $\lfloor M_{\text{opt}} \rfloor + 1$ are substituted into (45) to test which one achieves minimum μ. Note the optimal M must also satisfy (58).

Remarks:

1) Optimal values for M and γ are obtained asymptotically. For finite P and nonzero σ_n^2, M and γ can be optimized by maximizing μ.
2) When $P \to \infty$, we have $\mu \to 1$ and $P_{2b} \to 0$, eliminating any error floors. However, when P is finite, the residual channel-estimation error resulting from the finite-impulse response filter may result in an error floor in high SNR. It, however, decreases with increasing P.

3) In [6], it has been noticed that when P increases, the BER becomes a constant value, which can be obtained by substituting (38) into (20).
4) The maximum Doppler frequency $f_{\max}$ is much easier to estimate than the exact Doppler frequency f_D for a specific scenario because $f_{\max}$ depends on the maximum user speed.

B. NPDP Channels

Similar to the case of UPDP channels, during the nth symbol interval, we can obtain

$$\begin{aligned} m_{x_k x_k} &= E^s \sigma_k^2 + \sigma_n^2 \\ m_{y_k y_k} &= \mathbf{q}_k^H[n]\mathbf{R}_k^{-1}[n]\mathbf{q}_k[n], \quad \text{for} \quad k = 0, \ldots, L-1. \\ m_{x_k y_k} &= \sqrt{E^s} b[n] \mathbf{q}_k^H[n]\mathbf{R}_k^{-1}[n]\mathbf{q}_k[n]. \end{aligned} \tag{49}$$

Substituting (49) into (74), we obtain the closed-form BER of MRC under the LMMSE channel-estimation error. When $P \to \infty$ and $\sigma_n^2 \to 0$, we have

$$\begin{aligned} m_{y_k y_k} &= \sigma_k^2 - 2M f_D \frac{\sigma_n^2}{E^p} \\ m_{x_k y_k} &= \sqrt{E^s} b[n] \left(\sigma_k^2 - 2M f_D \frac{\sigma_n^2}{E^p} \right). \end{aligned} \tag{50}$$

Unfortunately, as (74) depends on $m_{x_k x_k}$, $m_{y_k y_k}$, $m_{x_k y_k}$, and PDP in a complicated way, a closed-form expression for the optimal M and γ cannot be derived. Instead, the optimal M and γ can be found numerically by minimizing the BER $P_{2b}(M, \gamma)$ using a 2-D search. However, numerical results in the next section show that (40) still holds in NPDP channels, and only a one-dimensional (1-D) search is needed to find γ_{opt}.

V. Simulation Results

We investigate the optimization of pilot symbols using different criteria in BPSK systems. Simulation is performed for both UPDP and NPDP channels. Jakes' model with $L = 3$ is used. In all of the simulations, we choose $P = 15$ and assume perfect knowledge of $\phi_l^c(\Delta t)$ and σ_n^2. The optimization using (12), (13), and (36) is denoted as "Finite P and finite σ_n^2," that using (39) with (62) is denoted as "$P \to \infty$ and finite σ_n^2," and that using (40) is denoted as "$P \to \infty$ and $\sigma_n^2 \to 0$." We also compare with the equipower training scheme with and without optimized M.

A. UPDP Channels

Fig. 5 shows the optimal pilot-symbol spacing M_{opt} under different conditions versus $\mathcal{E}/N_0$. In all cases, M_{opt} is insensitive to SNR but depends heavily on the Doppler frequency f_D. For $f_D = 0.05$, equipower training has $M_{\text{opt}} = 4$, and the other three require approximately $M_{\text{opt}} = 9$. For $f_D = 0.01$, M_{opt} is 8 for equipower training, and M_{opt} is about 49 for the other three. Note that the M (40) designed for the asymptotic case is also optimal when N is finite.

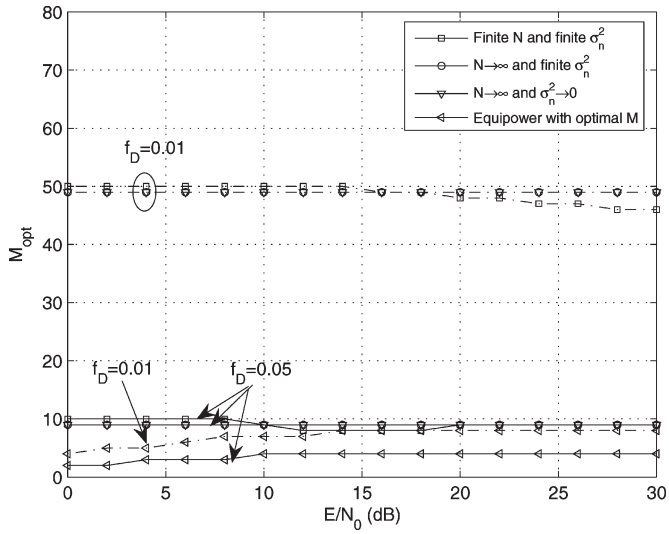

Fig. 5. Optimal pilot symbols spacing versus $\mathcal{E}/N_0$ with $L = 3$ and $P = 15$ in a UPDP channel.

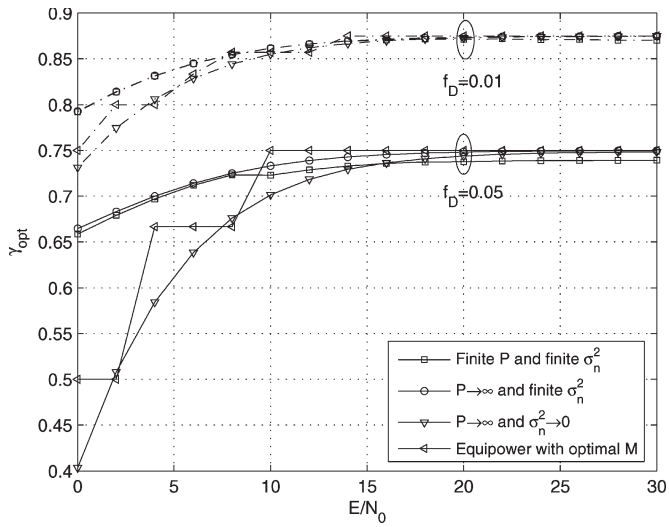

Fig. 6. Optimal γ versus $\mathcal{E}/N_0$ with $L = 3$ and $P = 15$ in a UPDP channel.

Fig. 6 presents the γ_{opt} of different criteria versus $\mathcal{E}/N_0$. For equipower training, M_{opt} is chosen using (46) instead of (48) by assuming perfect knowledge of noise variance. In all the cases, the γ in high SNR is larger than that in low SNR. This suggests that more power should be allocated to training in low SNR in order to combat the additive noise. In high SNR, γ becomes constant for all of the design criteria. On the other hand, γ decreases with the increase of f_D because in channels with higher Doppler spread, more training power should be used to combat the time selectivity.

Fig. 7 compares the BER results for different Doppler frequencies. The training schemes are optimized for each SNR value. The rake performance with perfect CSI (genie-aided) is used as a benchmark. We also compare the performance of equipower training with arbitrarily chosen M. In the simulation, we choose $M = 8$ for $f_D = 0.05$ and $M = 20$ for $f_D = 0.01$. The first three schemes perform almost identically for both of the Doppler rates. When $f_D = 0.01$, they perform

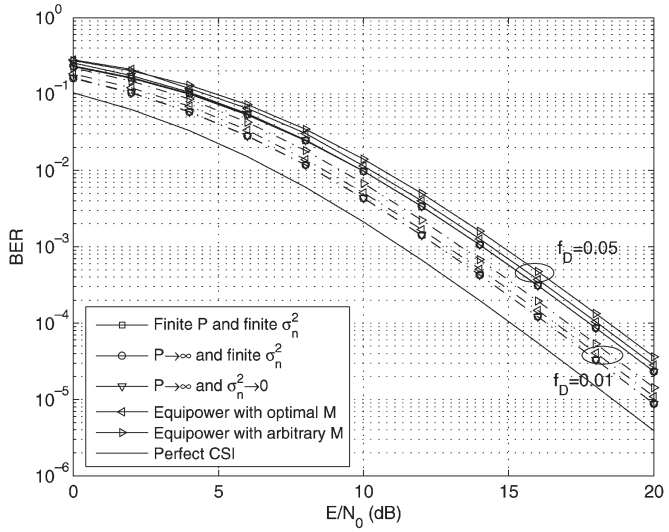

Fig. 7. BERs of different optimization criteria versus $\mathcal{E}/N_0$ with $L = 3$ and $P = 15$ in a UPDP channel.

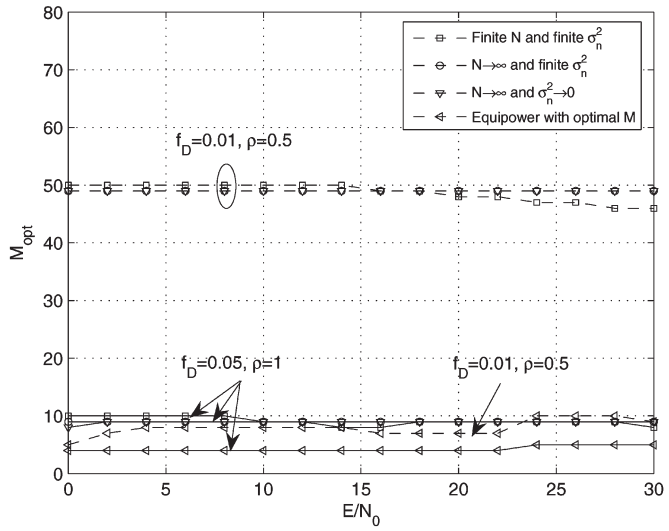

Fig. 8. Optimal pilot symbols spacing versus $\mathcal{E}/N_0$ with $L = 3$ and $P = 15$ in NPDP channels.

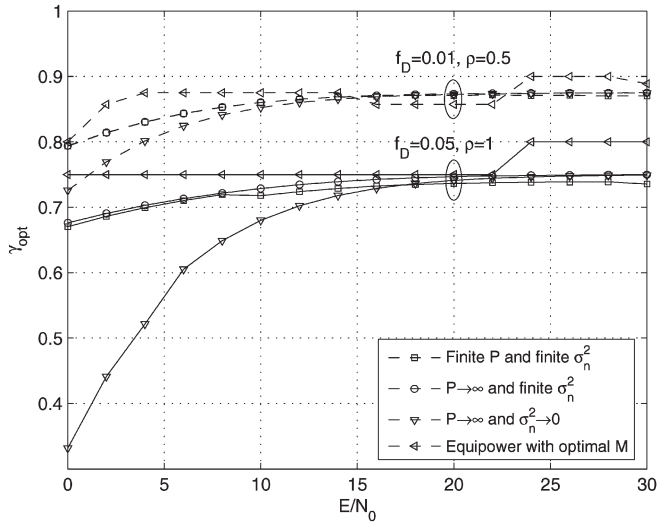

Fig. 9. Optimal γ versus $\mathcal{E}/N_0$ with $L = 3$ and $P = 15$ in NPDP channels.

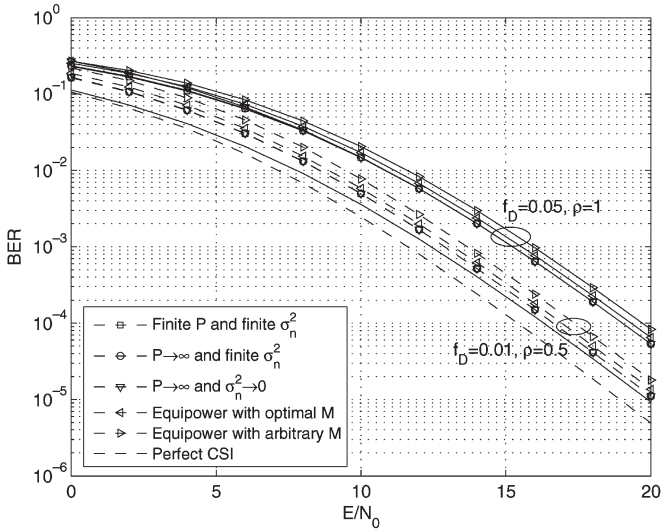

Fig. 10. BERs of different optimization criteria versus $\mathcal{E}/N_0$ with $L = 3$ and $P = 15$ in NPDP channels.

0.3 dB and 0.7 dB better than equipower training with and without optimized M, respectively, at a BER of 10^{-4}. However, they still lose 1.2 dB over the benchmark, which suggests the use of joint data detection and channel estimation. When f_D increases to 0.05, the performance gap between the first three schemes and the benchmark increases to 2.8 dB, due to time selectivity. Their performance gain over the equipower training scheme remains undiminished.

B. NPDP Channels

The EPDP channel model (3) is used as a representative sample of NPDP channels. We test different training schemes with $\rho = 0.5$ and $\rho = 1$. Fig. 8 gives the optimal M versus $\mathcal{E}/N_0$. The same results as that in UPDP channels are observed; M_{opt} is insensitive to $\mathcal{E}/N_0$ but is sensitive to f_D. Fig. 9 shows the γ_{opt} of different training schemes. While (41) is derived for UPDP channels, it also seems valid in NPDP channels. Comparing Fig. 6 with Fig. 9, we find that in low SNR, γ_{opt} for an NPDP channel is lower than that for a UPDP channel. However, in high SNR, γ_{opt} for both types of channels converge to (43). Finally, we present the BER of different training schemes in Fig. 10. Again, the first three schemes perform identically in all SNR. In the two cases with different f_D and ρ, they perform 0.3 dB and 0.7 dB better than equipower training with and without optimized M, respectively, at a BER of 10^{-4}. When $f_D = 0.05$ and $\rho = 1$, the performance gap between the first three schemes and the benchmark increases to 2.9 dB, which is caused by both the time- and frequency-selective channels. The results indicate that the asymptotic guidelines (41) and (42) still hold in NPDP channels.

VI. Conclusion

We have investigated the effect of channel-estimation errors on PSAM DS-CDMA systems over time-selective and frequency-selective fading channels and the optimization of

pilot symbols. A Wiener filter or an LMMSE channel estimator was used to estimate the time-varying channel. The asymptotic MSE of the LMMSE channel estimate was derived in closed form. In high SNR, the MSE does not depend on the Doppler spectrum. Closed-form BER expressions were also derived for MRC reception with Gaussian channel-estimation errors using the characteristic function method, which holds for both UPDP and NPDP channels. We optimized the pilot-symbol spacing and PDR by minimizing the BER. For UPDP channels, we obtained elegant asymptotic results for these two parameters, whereas their optimal values for NPDP channels can be obtained numerically. The results of this paper can be useful for designing PSAM systems and can also be extended to PCAM, Ricean channels, and large DS-CDMA systems analysis.

APPENDIX A

In this Appendix, we derive the MSE of the Wiener filter when $P \to \infty$. It cannot be derived in closed form via (16). Instead, we compute $\bar{\sigma}^2_{l,\Delta h}[m]$ in the frequency domain.

The Doppler spectrum of the channel is

$$S^c_l(f) = \mathcal{F}\left[\phi_l(\Delta t)\right] = \begin{cases} \sigma^2_l S^c(f), & |f| \le f_d \\ 0, & \text{otherwise} \end{cases} \tag{51}$$

where $S^c(f) = \mathcal{F}[\phi^c(\Delta t)]$. Typically, the spectrum for Jakes' model [9] is

$$S^c(f) = \begin{cases} \frac{1}{\pi f_d} \frac{1}{\sqrt{1-(f/f_d)^2}}, & |f| \le f_d \\ 0, & \text{otherwise.} \end{cases} \tag{52}$$

In the frequency domain, the MSE of the Wiener filter when $P \to \infty$ is given by [12, eq. (V.D.19)] as

$$\bar{\sigma}^2_{l,\Delta h}[m] = \sigma^2_l - \frac{1}{2\pi} \int_{-\pi}^{\pi} \frac{E^p \left|S_{d,p}(\omega)\right|^2}{E^p S_{d,d}(\omega) + \sigma^2_n} d\omega \tag{53}$$

where

$$S_{d,p}(\omega) = \sum_{n=-\infty}^{\infty} \phi^d_l[m - nM] e^{-\mathrm{j}\omega n} \tag{54}$$

and

$$S_{d,d}(\omega) = \sum_{n=-\infty}^{\infty} \phi^d_l[nM] e^{-\mathrm{j}\omega n}. \tag{55}$$

Because the sequence $\phi^d_l[nM]$ is the periodic sampling of the function $\phi^c_l(t)$ with sampling period MT_s, using [19, eq. (4.6)], we get

$$S_{d,d}(\omega) = \frac{1}{MT_s} \sum_{i=-\infty}^{\infty} S^c_l\left(\omega - i\frac{\omega_s}{M}\right) \tag{56}$$

where $\omega_s = 2\pi/T_s$ and $S_{d,d}(\omega)$ is a real function. Following the derivation of [19, eq. (4.6)], we can obtain

$$S_{d,p}(\omega) = S_{d,d}(\omega) e^{\mathrm{j}m\omega_s}. \tag{57}$$

Therefore, $|S_{d,p}(\omega)|^2 = S^2_{d,d}(\omega)$. To avoid aliasing, M should meet

$$\frac{\omega_s}{M} \ge 4\pi f_d \to M \le \frac{1}{2 f_d T_s}. \tag{58}$$

We define $f_D = f_d T_s$ as the normalized Doppler frequency. Note that if (58) is satisfied, we have

$$\sigma^2_l = \frac{M}{2\pi} \int_{-\pi}^{\pi} S_{d,d}(\omega) d\omega. \tag{59}$$

Substituting (56), (57), and (59) into (53), we obtain

$$\bar{\sigma}^2_{l,\Delta h} = \frac{1}{2\pi} \int_{-\omega_d}^{\omega_d} \frac{M S^d_l(\omega) \sigma^2_n}{E^p S^d_l(\omega) + M\sigma^2_n} d\omega \tag{60}$$

where $S^d_l(\omega) = S^c_l(\omega)/T_s$ and $\omega_d = 2\pi f_D$. We note that (60) does not depend on time index m, which is a necessary condition for optimizing pilot symbols in Section IV. The time index m is thus omitted. For Jakes' model, we have

$$S^d_l(\omega) = \begin{cases} \frac{2\sigma^2_l}{\omega_d} \frac{1}{\sqrt{1-(\omega/\omega_d)^2}}, & |\omega| \le \omega_d \\ 0, & \text{otherwise.} \end{cases} \tag{61}$$

Substituting (61), we get $\bar{\sigma}^2_{l,\Delta h}$ in closed form as

$$\bar{\sigma}^2_{l,\Delta h} = \begin{cases} c\left[\frac{\pi a}{2b} - \frac{2a^2}{b\sqrt{a^2-b^2}} \arctan\left(\frac{\sqrt{a^2-b^2}}{a+b}\right)\right], & a^2 > b^2 \\ c\left[\frac{\pi a}{2b} - \frac{a^2}{b\sqrt{b^2-a^2}} \ln \frac{a+b+\sqrt{b^2-a^2}}{a+b-\sqrt{b^2-a^2}}\right], & a^2 < b^2 \end{cases} \tag{62}$$

where

$$a = 2E^p\sigma^2_l, \quad b = M\omega_d\sigma^2_n, \quad c = b/(\pi E^p). \tag{63}$$

Specifically, in (60), when $\sigma^2_n \to 0$, we get an elegant result

$$\bar{\sigma}^2_{l,\Delta h} \simeq 2M f_D \frac{\sigma^2_n}{E^p}. \tag{64}$$

APPENDIX B

In BPSK, assuming $+1$ is transmitted, the error probability of the BPSK rake receiver is the probability that $P(D_R < 0)$, where

$$D_R = 2\Re\left\{\sum_{k=0}^{L-1} X_k Y^*_k\right\} = \sum_{k=0}^{L-1} X_k Y^*_k + X^*_k Y_k. \tag{65}$$

This is a special case of the general quadratic form

$$D_R = \sum_{k=0}^{L-1} \left(A|X_k|^2 + B|X_k|^2 + CX_k Y^*_k + C^* X^*_k Y_k\right) \tag{66}$$

where $A = 0$, $B = 0$, and $C = 1$ are constants and X_k and Y_k are a pair of correlated CGRVs. The L pairs $\{X_k, Y_k\}$ are mutually statistically independent.

From [5, App. B, pp. 943–945], the probability of error is given by

$$\begin{aligned} P_{2b} &= P(D_R < 0) \\ &= \int_{-\infty}^{0} p(D_R) dD_R \\ &= -\frac{1}{2\pi \mathrm{j}} \int_{-\infty+\mathrm{j}\varepsilon}^{+\infty+\mathrm{j}\varepsilon} \frac{\psi_{D_R}(\mathrm{j}v)}{v} dv \end{aligned} \tag{67}$$

where $\psi_{D_R}(\mathrm{j}v)$ is the characteristic function of D_R and ε is a small number to move the path of integration away from the singularity at $v = 0$.

Because D_R is the sum of L nonidentically distributed independent variables, the characteristic function of D_R can be factored into the product of L characteristic functions. Let d_k be

$$d_k = X_k Y_k^* + X_k^* Y_k, \quad k = 0, 1, \cdots, L-1. \tag{68}$$

Because X_k and Y_k have zero mean, the characteristic function of d_k is given by [5, p. 944]

$$\psi_{d_k}(\mathrm{j}v) = \frac{v_{k1} v_{k2}}{(v + \mathrm{j}v_{k1})(v - \mathrm{j}v_{k2})} \tag{69}$$

where the parameters v_{k1} and v_{k2} depend on $m_{x_k x_k}$, $m_{y_k y_k}$, and $m_{x_k y_k}$ as in (22), which are not identical for different ks, and we get

$$\begin{aligned} v_{k1} &= \sqrt{w_k^2 + \frac{1}{4\left(m_{x_k x_k} m_{y_k y_k} - m_{x_k y_k}^2\right)}} - w_k > 0 \\ v_{k2} &= \sqrt{w_k^2 + \frac{1}{4\left(m_{x_k x_k} m_{y_k y_k} - m_{x_k y_k}^2\right)}} + w_k > 0 \\ w_k &= \frac{m_{x_k y_k}}{2\left(m_{x_k x_k} m_{y_k y_k} - m_{x_k y_k}^2\right)}. \end{aligned} \tag{70}$$

The characteristic function of D_R is therefore

$$\psi_{D_R}(\mathrm{j}v) = \prod_{k=0}^{L-1} \psi_{d_k}(\mathrm{j}v). \tag{71}$$

To evaluate the error probability in (67), we derive a partial fraction expansion of $\psi_{D_R}(\mathrm{j}v)/v$ as

$$\begin{aligned} \frac{\psi_{D_R}(\mathrm{j}v)}{v} &= \frac{\prod_{k=0}^{L-1} \psi_{d_k}(\mathrm{j}v)}{v} \\ &= \frac{1}{v} + (-1)^L \sum_{k=0}^{L-1} \frac{v_{k2}}{v_{k1} + v_{k2}} \\ &\quad \prod_{l=0, l\neq k}^{L-1} \frac{v_{l1} v_{l2}}{(v_{k1} - v_{l1})(v_{k1} + v_{l2})} \frac{1}{v + \mathrm{j}v_{k1}} \\ &\quad + (-1)^L \sum_{k=0}^{L-1} \frac{v_{k1}}{v_{k1} + v_{k2}} \\ &\quad \prod_{l=0, l\neq k}^{L-1} \frac{v_{l1} v_{l2}}{(v_{k2} + v_{l1})(v_{k2} - v_{l2})} \frac{1}{v - \mathrm{j}v_{k2}}. \end{aligned} \tag{72}$$

From complex variable theory [20], we know that

$$\int_{-\infty+\mathrm{j}\varepsilon}^{+\infty+\mathrm{j}\varepsilon} \frac{1}{v + \mathrm{j}\alpha} dv = 2\pi \mathrm{j}\,(1 - u(\alpha)) \tag{73}$$

for real α. The error probability of (67) can therefore be evaluated as

$$\begin{aligned} P_{2b} &= -\frac{1}{2\pi \mathrm{j}} \int_{-\infty+\mathrm{j}\varepsilon}^{+\infty+\mathrm{j}\varepsilon} \frac{\psi_{D_R}(\mathrm{j}v)}{v} dv \\ &= (-1)^{L+1} \sum_{k=0}^{L-1} \frac{v_{k1}}{v_{k1} + v_{k2}} \\ &\quad \times \prod_{l=0, l\neq k}^{L-1} \frac{v_{l1} v_{l2}}{(v_{k2} + v_{l1})(v_{k2} - v_{l2})}. \end{aligned} \tag{74}$$

REFERENCES

[1] P. Chaudhury, W. Mohr, and S. Onoe, "The 3GPP proposal for IMT-2000," *IEEE Commun. Mag.*, vol. 37, no. 12, pp. 72–81, Dec. 1999.

[2] P. Schramm and R. Muller, "Pilot symbol assisted BPSK on Rayleigh fading channels with diversity: Performance analysis and parameter optimization," *IEEE Trans. Commun.*, vol. 46, no. 12, pp. 1560–1563, Dec. 1998.

[3] P. Schramm, "Analysis and optimization of pilot-channel-assisted BPSK for DS-CDMA systems," *IEEE Trans. Commun.*, vol. 46, no. 9, pp. 1122–1124, Sep. 1998.

[4] M. Benthin and K.-D. Kammeyer, "Influence of channel estimation on the performance of a coherent DS-CDMA system," *IEEE Trans. Veh. Technol.*, vol. 46, no. 2, pp. 262–268, May 1997.

[5] J. G. Proakis, *Digital Communications*, 4th ed. New York: McGraw-Hill, 2001.

[6] J. Cavers, "An analysis of pilot symbol assisted modulation for Rayleigh fading channels," *IEEE Trans. Veh. Technol.*, vol. 40, no. 4, pp. 686–693, Nov. 1991.

[7] W. Li and N. Beaulieu, "Optimization of pilot symbol assisted BPSK with diversity," in *Proc. IEEE Pacific Rim Conf. Commun., Comput. and Signal Process.*, Aug. 2003, vol. 2, pp. 744–747.

[8] W. Phoel and M. Honig, "Performance of coded DS-CDMA with pilotassisted channel estimation and linear interference suppression," *IEEE Trans. Commun.*, vol. 50, no. 5, pp. 822–832, May 2002.

[9] W. C. Jakes, Jr., *Microwave Mobile Communications*. New York: Wiley, 1974.

[10] E. Biglieri, J. Proakis, and S. Shamai, "Fading channels: Information-theoretic and communications aspects," *IEEE Trans. Inf. Theory*, vol. 44, no. 6, pp. 2619–2692, Oct. 1998.

[11] T. Eng and L. B. Milstein, "Coherent DS-CDMA performance in Nakagami multipath fading," *IEEE Trans. Commun.*, vol. 43, no. 234, pp. 1134–1143, Feb.–Apr. 1995.

[12] H. V. Poor, *An Introduction to Signal Detection and Estimation*, 2nd ed. New York: Springer-Verlag, 1994.

[13] S. Ohno and G. B. Giannakis, "Capacity maximizing MMSE-optimal pilots for wireless OFDM over frequency-selective block," *IEEE Trans. Inf. Theory*, vol. 50, no. 9, pp. 2138–2145, Sep. 2004.

[14] G. L. Stuber, *Principles of Mobile Communication*, 2nd ed. Norwell, MA: Kluwer, 2001.
[15] B. Xia and J. Wang, "Effect of channel-estimation error on QAM systems with antenna diversity," *IEEE Trans. Commun.*, vol. 53, no. 3, pp. 481–488, Mar. 2005.
[16] *Universal mobile telecommunications system (UMTS): Spreading and modulation (FDD), 3GPP TS 25.213 version 6.2.0 Release 6, 2005-03*. [Online]. Available: http:www.3gpp.org
[17] A. Naguib and A. Paulraj, "Performance of wireless CDMA with Mary orthogonal modulation and cell site antenna arrays," *IEEE J. Sel. Areas Commun.*, vol. 14, no. 9, pp. 1770–1783, Dec. 1996.
[18] C. Mun, M.-S. Choi, and H.-K. Park, "Performance of 2-D RAKE receiver in a correlated frequency-selective Nakagami-fading," *IEEE Trans. Veh. Technol.*, vol. 50, no. 5, pp. 1312–1317, Sep. 2001.
[19] A. V. Oppenheim, R. W. Schafer, and J. R. Buck, *Discrete-Time Signal Processing*, 2nd ed. Englewood Cliffs, NJ: Prentice-Hall, Feb. 1999.
[20] L. Serge, *Complex Analysis*, 3rd ed. New York: Springer-Verlag, 1993.

Tao Cui (S'04) received the B.Eng. degree in information engineering from Xi'an Jiaotong University, Xi'an, China, in 2003 and the M.Sc. degree from the University of Alberta, Edmonton, AB, Canada, in 2005. He is currently working toward the Ph.D. degree at the Department of Electrical Engineering, California Institute of Technology, Pasadena.

His research interests include communication theory, broadband wireless communications, space–time coding, multiple-input–multiple-output systems, and wireless networks.

Mr. Cui was a recipient of postgraduate scholarships from the Alberta Ingenuity Fund and the Alberta Informatics Circle of Research Excellence (iCORE).

Chintha Tellambura (M'97–SM'02) received the B.Sc. degree (with first-class honors) from the University of Moratuwa, Moratuwa, Sri Lanka, in 1986, the M.Sc. degree in electronics from the University of London, London, U.K., in 1988, and the Ph.D. degree in electrical engineering from the University of Victoria, Victoria, BC, Canada, in 1993.

He was a Postdoctoral Research Fellow with the University of Victoria (1993–1994) and the University of Bradford (1995–1996). From 1997 to 2002, he was with Monash University, Melbourne, Australia. He is currently a Professor with the Department of Electrical and Computer Engineering, University of Alberta, Edmonton, AB, Canada. His research interests include coding, communication theory, modulation, equalization, and wireless communications.

Prof. Tellambura was the Chair of the Communication Theory Symposium in Globecom'05, which was held in St. Louis, MO. He is an Associate Editor for both the IEEE TRANSACTIONS ON COMMUNICATIONS and the IEEE TRANSACTIONS ON WIRELESS COMMUNICATIONS.